

## Numerical and experimental study of heat transfer in a cubic cavity with a PCM in a vertical heated wall

S. Moreno<sup>a</sup>, J.F. Hinojosa<sup>a,\*</sup>, I. Hernández-López<sup>a</sup>, J. Xaman<sup>b</sup>

<sup>a</sup> Universidad de Sonora (UNISON), Blvd. Rosales y Luis Encinas, Hermosillo, CP 83000 Sonora, Mexico

<sup>b</sup> Nacional de México / CENIDET, prol. Av. Palmira S/N. Col. Palmira, Cuernavaca, Morelos CP 62490, Mexico



### HIGHLIGHTS

- A detailed transient numerical analysis of heat transfer is reported in a cavity with PCM in a wall.
- An experimental setup was built to validate the mathematical model and numerical methodology.
- A parametric study was conducted to determine the effect on Nusselt number and average temperature.
- The PCM store heat is extended to 120 min as the PCM thickness is increased from 0.0005 m to 0.002 m.
- The buoyancy effect on the PCM wall produces an uneven temperature at the shared wall.

### ARTICLE INFO

**Keywords:**

Natural convection  
Experimental and numerical study  
PCM modeling

### ABSTRACT

In this work, a transient numerical and experimental study is presented, focused on describing the heat transfer in a cavity filled with air, which has one vertical wall with a phase change material (PCM). The wall with PCM was exposed to constant heat flux, whereas the opposite vertical wall was kept at a constant temperature. For the theoretical study, a model for heat transfer was proposed and solved using computational fluid dynamics software. The enthalpy method was used to simulate the phase change in the PCM. For the experimental study, five temperature profiles were obtained for air, one for PCM, and at different points of shared wall between PCM and air. A comparison was made, between, experimental and numerical data, to determine the predictive capacity of the model. Besides, numerical results of the liquid fraction in the PCM were compared with data reported in the specialized literature. It was found that the enthalpy method was adequate to study proposed in this study. The numerical temperature fields and flow patterns in the air were analyzed, as well as the evolution of the liquid fraction in the PCM. With the validated model, a parametric study was conducted to quantify the effect of Rayleigh number and PCM thickness on Nusselt number and the average air temperature. It was found that the use of the PCM decreased the heat transfer to the air. The comparison with the case without PCM indicated that Nusselt number values reduced between 66.80 and 75.47%.

### 1. Introduction

According to world population prospects [1], in the last ten years world population has grown up 1.24 percent every year. The prediction for the coming years is that by 2050, the world population will reach 9.8 billion people, which leads to a global increase in primary total energy supply between 27 and 61 percent [2]. One way to reduce this impact is by having a proper energy administration. About 35 percent of total energy supply is used for thermal requirements in buildings, because of this studying proper energy administration in buildings becomes essential.

For years, many passive technologies for energy administration improvement in buildings have been developed. These technologies are divided into three major groups: solar and heat protection (decreasing heat absorption), heat modulation (modifying heat gains), and heat dissipation (removing of internal heat) [3]. However, using phase change materials (PCM) in walls is a heat moderation technic, which consists of storing thermal energy as latent heat in the PCM. They help to reduce energy consumption, delay the load of thermal peaks, facilitate temperature control in building components, and extend their durability [4–6].

One way of modeling the effect of phase change materials on heat

\* Corresponding author.

E-mail address: [fhinojosa@iq.uson.mx](mailto:fhinojosa@iq.uson.mx) (J.F. Hinojosa).

<b>Nomenclature</b>		$\mu$	Dynamic viscosity (Pa·s)
$A_{mush}$	Mushy zone constant ( $\frac{\text{kg}}{\text{m}^3\text{s}}$ )	$\rho$	Density ( $\frac{\text{kg}}{\text{m}^3}$ )
$C_p$	Specific heat ( $\frac{\text{J}}{\text{kgK}}$ )	$\tau$	Stress tensor
$f$	Liquid fraction (-)	$\delta$	PCM thickness (m)
$g$	Gravity ( $\frac{\text{m}}{\text{s}^2}$ )	$\lambda$	Thermal conductivity (W/m·K)
$h$	Sensible heat ( $\frac{\text{kJ}}{\text{kg}}$ )	<i>Subscripts</i>	
$H$	Enthalpy ( $\frac{\text{kJ}}{\text{kg}}$ )	$X, Y, Z$	Coordinates
$\Delta H$	Latent heat ( $\frac{\text{kJ}}{\text{kg}}$ )	$c$	Cold wall
$L$	Length (m)	$l$	Liquid PCM
$Nu$	Nusselt number (-)	$s$	Solid PCM
$Ra$	Rayleigh number (-)	$ref$	Reference value
$P$	Pressure (Pa)	$eff$	Effective
$q''$	Heat flux ( $\frac{\text{W}}{\text{m}^2}$ )	$avg$	Average
$t$	Time (s)	<i>Abbreviations</i>	
$T$	Temperature (K)	$PCM$	Phase change material
$T_c$	Cold surface temperature (K)	$PISO$	Pressure-implicit with splitting of operators
$X, Y, Z$	Cartesian coordinates	$MUSCL$	Monotonic upwind scheme for conservation laws
$v$	Velocity (m/s)	$MAPE$	Mean absolute percentage error
<i>Greek symbols</i>		$RMSE$	Root mean square error
$\beta$	Coefficient of thermal expansion ( $\frac{1}{\text{K}}$ )		

transfer in rooms and offices is using a scaled cavity, which permits to control of relevant parameters and to obtain reproducible results. The previous investigations of heat transfer in rectangular cavities with PCM materials are categorized and described briefly next.

#### (a) Numerical studies in rectangular cavities with PCM materials.

Ye [7] numerically studied the effect of different aspect ratios, from 0.1 to 10, for rectangular cavities with a PCM. The melting speed increases proportionally with the aspect ratio, especially for aspect ratios greater than 1. Initially, the phenomenon of heat transfer by conduction is dominant, then there is a transition from conduction to convection, and in the end, the convective phenomenon is dominant. Bondareva and Sheremet [8] analyzed the interaction of natural convection and melting of phase change material inside a square cavity with a local heater of volumetric heat generation. The effects of heat generation intensity and buoyancy force were analyzed. Li *et al.* [9] studied the

appropriate geometric design of the PCM enclosure to augment natural convection passively. It was found that tilting the top wall accelerates heat transfer and latent heat storage due to beneficial alterations to natural convection within the molten PCM. Bouhal *et al.* [10] conducted a numerical study in three differentially heated cavities. These cavities were one without fins, one with a rectangular fin and the other with a triangular fin. The mathematical model was based on the enthalpy method. Using fins decreases the time it takes for the PCM to melt, for the rectangular fins it decreased from 35 min to 32 min. Wang *et al.* [11] simulated a south-faced wall with a PCM layer in sunny hot summer weather in Shanghai city. It was found that compared to the wall without the PCM layer, the best performance of the PCM wall after optimization can reduce the heat flow by 34.9%.

Iten *et al.* [12] developed two mathematical models for the simulation of air-thermal storage unit system. The mathematical models were based on the enthalpy method and the effective specific heat method. Both models showed approximately the same percentage of

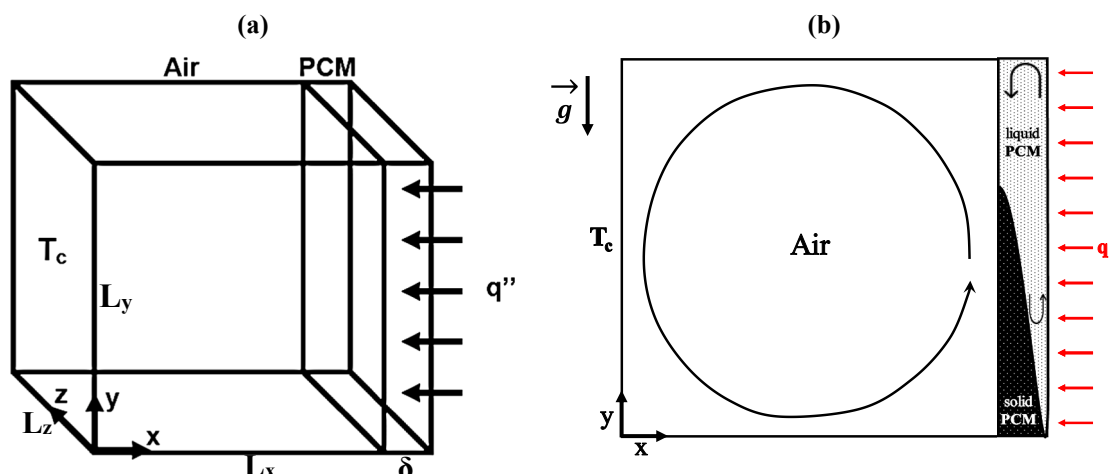
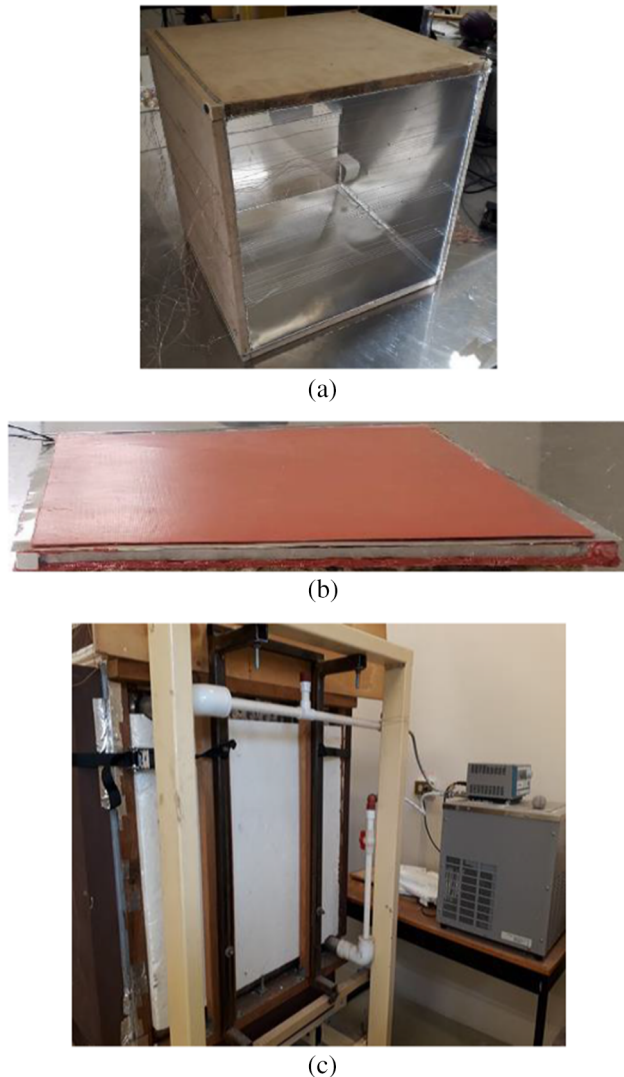


Fig. 1. Scheme of the physical model: (a) thermal system configuration and (b) basic fluids motion in the system.



**Fig. 2.** Experimental setup. (a) Air-filled cavity, (b) PCM-filled cavity with a flexible electrical heater, and (c) Thermostatic bath with a heat exchanger (isothermal wall).

error of 0.4% (discharge) and 1.6% (load). Li *et al.* [13] theoretically studied the thermal behavior of a Trombe wall with PCM. The results showed that adding PCM to the traditional Trombe wall can improve the indoor temperature and reduce the thermal load. Xaman *et al.* [14] carried out a numerical simulation of a solar chimney system. They tested three different absorbers. The model used for heat transfer in the

PCM was based on the specific effective heat method. The copper configuration was the one with the highest mass flow. Fadl and Eames [15] studied numerically the effect of the mushy zone constant value on the phase change characteristics of lauric acid. They noticed that smaller values ( $< 10^5$ ) reached unrealistic predictions and higher values ( $> 10^6$ ) resulted in a delayed prediction of the process. Zhang [16] analyzed modified computational methods, which use a two-dimensional effective heat capacity model for predicting the transient heat transfer process of the building envelopes outfitted with phase change materials.

Souayfane *et al.* [17] reported a simplified model for the melting of a PCM in the presence of natural convection and thermal radiation. The proposed simplified model is simple to implement, and its simulations run significantly faster than those of CFD models and the LBM-DOM model. Bhamare *et al.* [18] made a 3D numerical simulation in a full-scale room with PCM in the roof. The authors found a significant reduction in daily heat gain can be achieved by providing the inclination to the PCM layer. Sadeghi *et al.* [19] studied the effect of charging and discharging of multilayers PCMs in coaxial cylinders with time-periodic boundary conditions, they enhanced the amount of energy saved within the PCM from 23.28% to 41.67% in the case of one layer compared to the case of three layers.

Another strategy to simulate the phase change is with the deformed grid method, which helps to track the phase change front, and is controlled by the Stefan condition. Mehtyan *et al.* [20] studied the effect of conjugate wall thickness, inclination angle, and the porous layer thickness on the phase change heat transfer of PCM. For their configuration, with an angle of 45°, the melting rate was the highest.

(b) Experimental studies in rectangular cavities with PCM materials.

Kamkari *et al.* [21] investigated the thermal and hydraulic behavior of a phase change material within a rectangular cavity inclined at different angles (0°, 45°, and 90°). Decreasing the inclination leads to a considerable improvement in the transport of energy from the hot wall to the PCM. Jin *et al.* [22] evaluated the thermal performance of a PCM into three different wall locations within the cavity of a typical North American residential wall system. Soares *et al.* [23] evaluated the heat transfer through small thermal energy storage units filled with different phase change materials. The authors concluded the dominant transport mechanism is conduction, but convection cannot be neglected. Kara [24] investigated the thermal performance of the phase change material (PCM) walls. It was found that the daily ratio of the solar energy gain provided by the walls to the heat load of the test room varied from 12% to 25%. Wang *et al.* [25] evaluated the year-round applicability of a kind of composite-PCMs wall in a full-scale room. It was observed a reduction of 24.32% of the cooling load under summer conditions. Gounni and Alami [26] carried out an experimental study to determine the most appropriate configuration to place PCM. Placing the PCM near

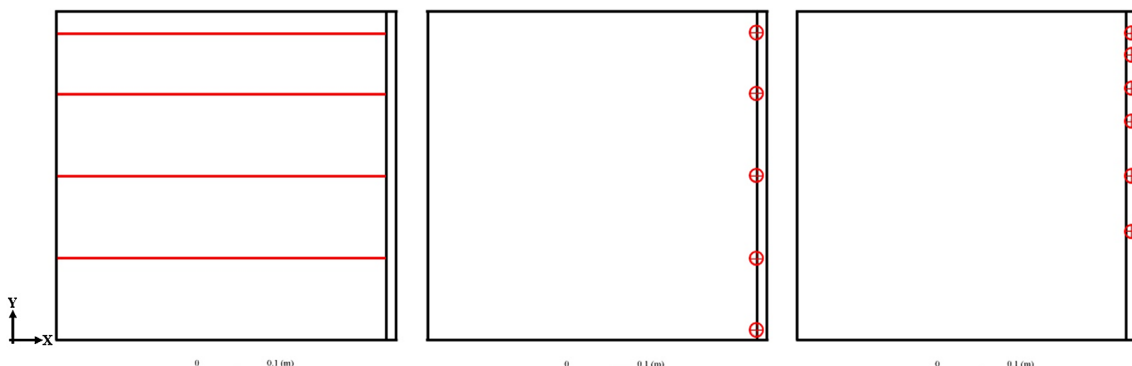


**Fig. 3.** Location of thermocouples in the experimental cavity.

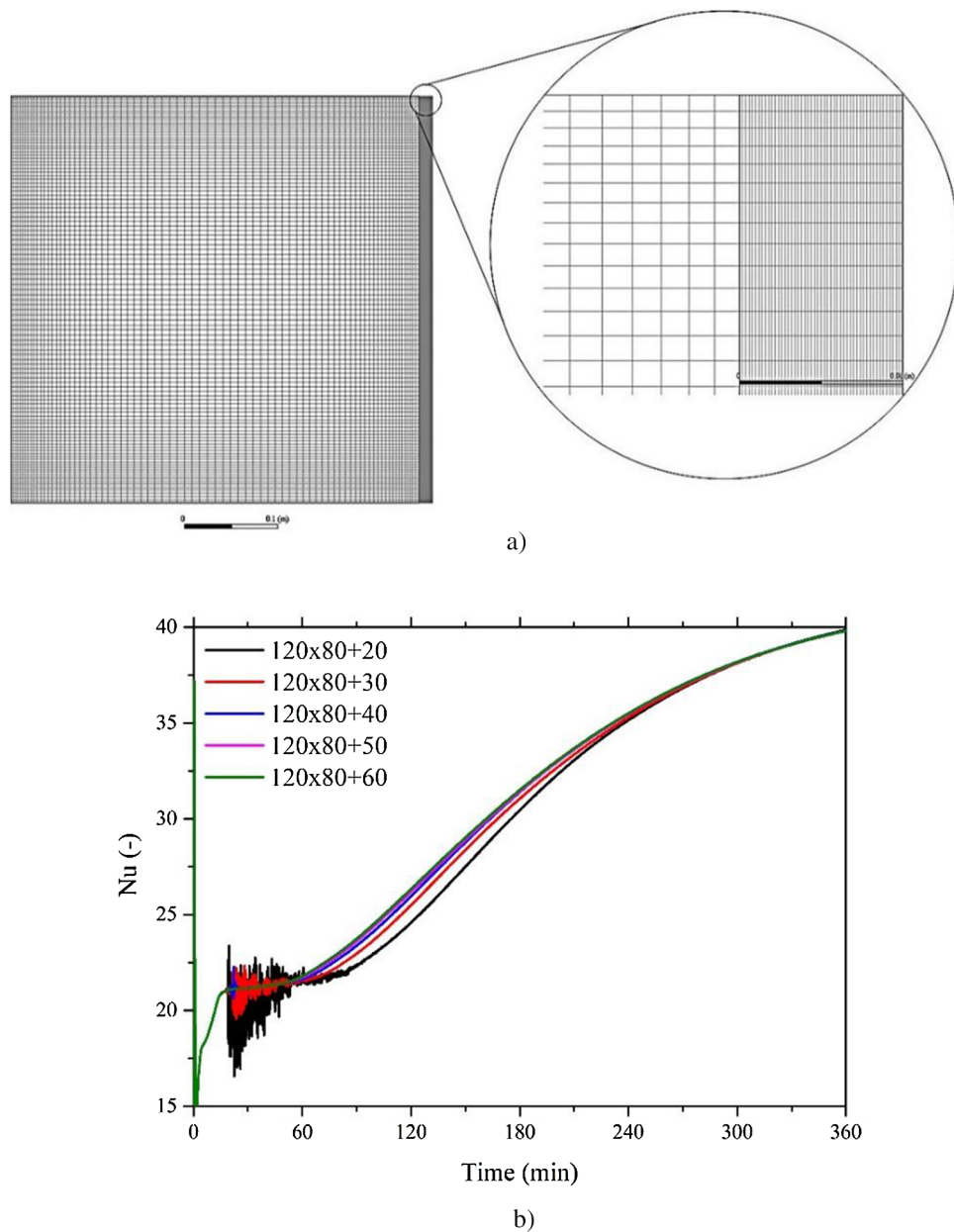


**Fig. 4.** a) Computational mesh, b) Average Nusselt number evolution of shared wall.

**Table 1**  
Temporary independence study.

Time step (s)	Average Nusselt number	Liquid fraction ( $f$ )	Percentage Difference for Nu	Percentage Difference for $f$
0.10	43.92	0.43	–	–
0.20	43.92	0.43	0.01%	0.18%
0.50	43.94	0.43	0.03%	0.66%
0.75	43.96	0.43	0.05%	1.00%
1.00	43.98	0.44	0.05%	1.59%
2.00	44.32	0.47	0.76%	7.21%

the heat source is the best option to decrease the peak heat flow value and in terms of configurations.

Ambarita *et al.* [27] experimentally investigated the fusion and solidification process in two different PCM. The experiment was performed in a glass cavity. As a result, it was found that the melting process starts from the upper part closer to the hot wall, but

solidification starts at the bottom part closer to the cold wall. David *et al.* [28] made an experimental investigation to characterize the natural convection heat transfer along with panels that contain a PCM. It was found that the phase change is characterized by a first dynamic stage, a wall temperature slowdown/retrogression process, and a second dynamic stage. Sun *et al.* [29] conducted an experimental study to figure out the heat transfer mechanisms during the melting process of a PCM in rectangular panels. Because of the presence of natural convection, a melting time reduction ranging from 18.8% to 50.8% was observed. Sun *et al.* [30] experimentally studied the heat transfer rate enhancement caused by natural convection of PCMs undergoing melting. The presence of natural convection reduced the time required for complete melting by approximately 45% for vertical heat transfer.

(c) Numerical and experimental studies in closed cavities with PCM materials in the walls.

Labibi *et al.* [31] theoretically and experimentally studied the effect

**Table 2**  
Materials properties.

Material	Density (kg/m <sup>3</sup> )	Thermal conductivity (W/m K)	Specific heat (J/kg K)	Viscosity (kg/m s)	Temperature(°C)	Latent heat (kJ/kg)	Thermal expansion coefficient (1/K)
Solid PCM	940	0.25	1770		28.6	202	
Liquid PCM	850	0.15	1940	$3.74 \times 10^{-3}$	29.4		
Air	1.204	0.2514	1007	$1.825 \times 10^{-5}$			0.0033
Aluminum	2719	202.4	871				

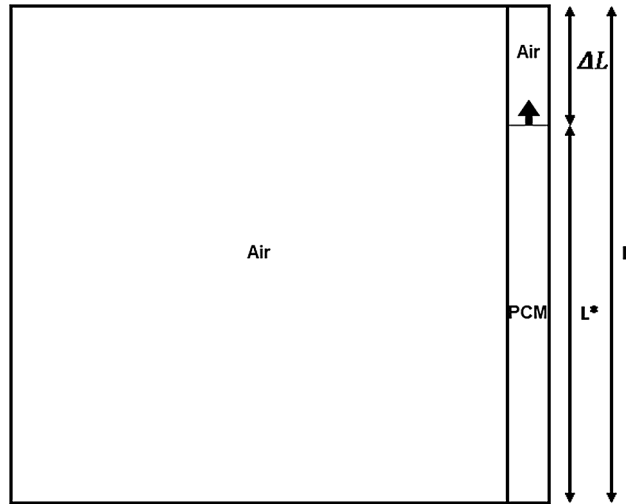


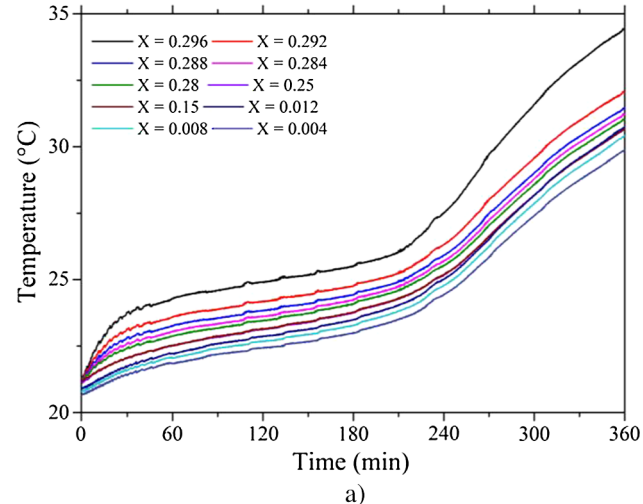
Fig. 5. PCM expansion.

of loading on a phase change material on an air cavity. For the air, they used a cubic cavity of  $10\text{ cm} \times 10\text{ cm} \times 10\text{ cm}$  and for the PCM a cavity with a thickness of 1 cm. They proposed an effective density, which reduces the standard deviation between experimental and numerical results from 2 to 0.66 and 1.4 to 0.74 for the PCM and the air, respectively. Elarga *et al.* [32] investigated the thermal performances of a PCM integrated into a roof space. Three different solutions were applied to a roof monitored under summer climatic conditions. Experimental results showed a reduction of the ongoing heat peak load between 13% and 59% depending on the PCM typology.

There are some methods for the analysis of convection inside enclosures, one of them is using particle image velocimetry (PIV). Corvaro *et al.* [33–35] used PIV to experimentally obtain velocity contours and streamlines in a square cavity filled with air, varying the gravity vector relative position, and the Rayleigh number. Besides, they solved a mathematical model for the movement, and the radiative and convective heat transfer, with a good agreement with experimental data.

A new trending in phase change materials is rising: nano encapsulated PCM. Ghalambaz *et al.* [36] for the study they used a differentially heated square cavity filled with core-shell particles with PCM in the core, they show that the fusion temperature of the particles is the key factor affecting the heat transfer enhancement of the nano encapsulated phase change material in the natural convection flow. Hajjar *et al.* [37] did the same technic but considering a time-periodic temperature, they probed that increasing the volume fraction of nanoparticles enhances the average Nusselt number. Mehryan *et al.* [38] investigated the natural convection of AgMgO/water in a porous enclosure, noticing that dispersing nanoparticles in the water strongly decreases the transport of heat through two phases of the porous enclosure. Chamkha *et al.* [39] showed that the solid-liquid interface and the liquid fraction are significantly affected by the volume fraction of nanoparticles and the thermal conductivity parameter.

The above literature analysis shows the absence of detailed experimental and numerical study of heat transfer in a thermal system formed for two coupled cavities, one filled with a PCM material and the



a)

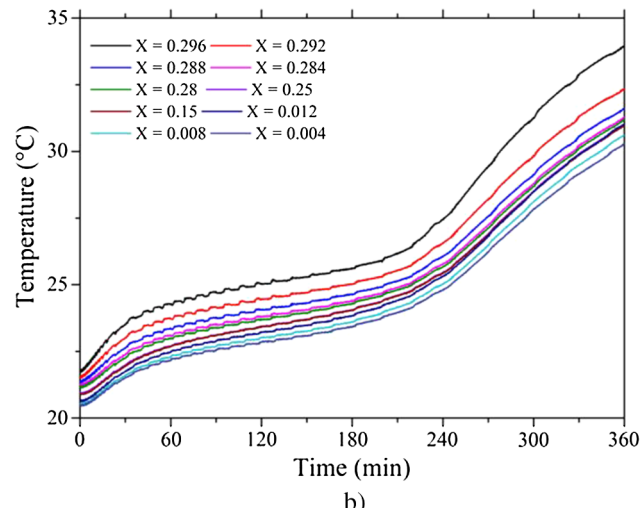


Fig. 6. Temperature evolution along X axis. a)  $Y = 0.15\text{ m}$ ,  $Z = 0.15\text{ m}$  and b)  $Y = 0.15\text{ m}$ ,  $Z = 0.225\text{ m}$ .

other with air. This configuration is relevant to analyze the effect of phase change materials in walls on heat transfer in rooms and offices. Considering the above, the objective of this study was to conduct a detailed analysis (numerical and experimental) of heat transfer in a scaled coupled cavities thermal system to better understand the phenomena. The enthalpy method was selected to make a theoretical study. An experimental setup was built to obtain five experimental temperature profiles for air and one in PCM. The experimental data were used to validate the proposed mathematical model a numerical methodology. It was verified a two-dimensional behavior in the thermal system. Then, the experimental profiles were compared with predicted numerical results, and the deviation was obtained. Finally, with the validated model, a parametric study was made to determine the effect of applied heat flux (Rayleigh number), presence of PCM and PCM

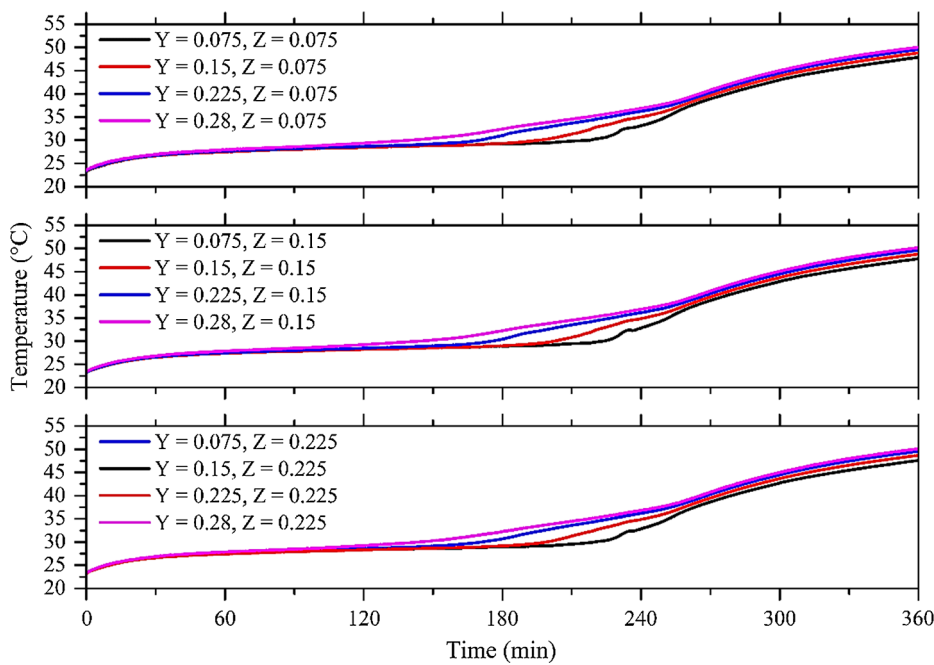


Fig. 7. Temperature evolution at the shared wall.

thickness on heat transfer coefficients (Nusselt number), the liquid fraction of PCM and mean air temperature.

## 2. Physical and mathematical model

### 2.1. Physical model

This study was performed using two coupled closed cavities, as shown in Fig. 1a. The dimensions were  $L_x = L_y = L_z = 0.3$  m on air-filled cavity and  $\delta = 0.01$  m,  $L_y = L_z = 0.3$  m on PCM filled cavity. For the air-filled cavity, one of its vertical walls ( $x = 0$  m) was kept at a constant temperature  $T_c$ , whereas the remaining walls were assumed adiabatic. For PCM filled cavity, one vertical wall ( $x = L_x + \delta = 0.31$  m) received a uniform and constant heat flux. Both cavities share one vertical wall ( $x = 0.3$  m). Under the above thermal conditions, the basic physical model for fluids flow is shown in Fig. 1b.

### 2.2. Mathematical model

For the mathematical model, the following considerations were taken:

- Transient state.
- Air and melted PCM behave as a Newtonian fluid.
- Laminar flow regime.
- Impermeable and no-slip condition at walls.
- The Boussinesq approximation is valid for air.
- Thermal radiation is negligible.
- Two-dimensional behavior.
- PCM is homogeneous and isotropic.
- The density, thermal conductivity, and specific heat of PCM changes with change in phase.

With the above assumptions, governing equations were [40,41]:

Continuity for air and PCM:

$$\frac{\partial \rho}{\partial t} + \vec{\nabla} \cdot (\rho \vec{v}) = 0 \quad (1)$$

Momentum for air:

$$\frac{\partial}{\partial t}(\rho \vec{v}) + \nabla \cdot (\rho \vec{v} \vec{v}) = -\nabla P + \nabla \cdot (\vec{\tau}) + \rho_{ref} \beta(T - T_{ref}) \vec{g} \quad (2)$$

Momentum for PCM:

$$\frac{\partial}{\partial t}(\rho \vec{v}) + \nabla \cdot (\rho \vec{v} \vec{v}) = -\nabla P + \nabla \cdot (\vec{\tau}) + \rho \vec{g} + \vec{F} \quad (3)$$

Energy for air and PCM:

$$\frac{\partial}{\partial t}(\rho H) + \nabla \cdot (\rho \vec{v} H) = \nabla \cdot (\lambda \nabla T) \quad (4)$$

To deal with phase change, the enthalpy method was chosen [42]. In this method, enthalpy is computed as the sum of sensible heat,  $h$ , and latent heat,  $\Delta H$ .

$$H = h + \Delta H \quad (5)$$

Where sensible heat is given by:

$$h = h_{ref} + \int_{T_{ref}}^T C_p dT \quad (6)$$

And latent heat by:

$$\Delta H = fL \quad (7)$$

where  $h_{ref}$ ,  $T_{ref}$ ,  $C_p$ ,  $L$ ,  $f$  correspond to reference enthalpy, reference temperature, specific heat, latent heat, and liquid fraction, respectively. The liquid fraction is defined as:

$$f = \begin{cases} 0 & T < T_s \\ \frac{T - T_s}{T_l - T_s} & T_s \leqslant T \leqslant T_l \\ 1 & T > T_l \end{cases} \quad (8)$$

Replacing Eqs. (6) and (7) into (5), then Eq. (8):

$$H = \begin{cases} \int_{T_s}^T C_p dT & T < T_s \\ \frac{T - T_s}{T_l - T_s} L & T_s \leqslant T \leqslant T_l \\ \int_{T_l}^T C_p dT + L & T > T_l \end{cases} \quad (9)$$

In summary, the temperature is solved iterating between energy Eq. (4) and the liquid fraction Eq. (8). In this method, the phase change is not tracked explicitly; otherwise, a porosity formulation is used, which

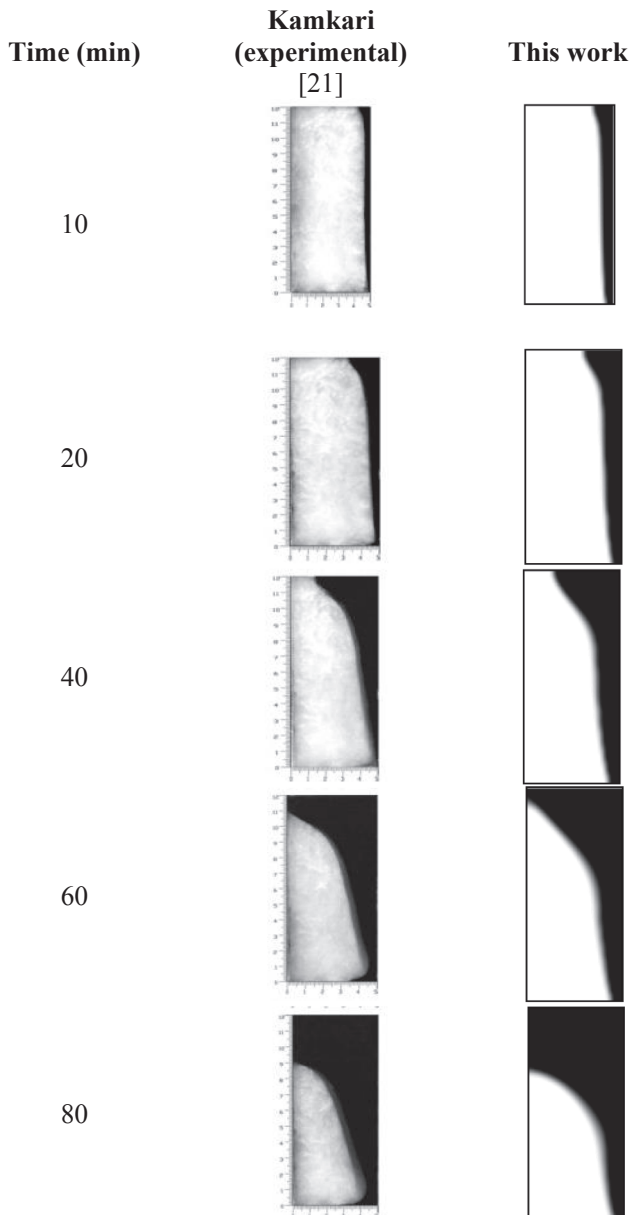


**Fig. 8.** Theoretical and experimental comparison of the evolution of the liquid phase.

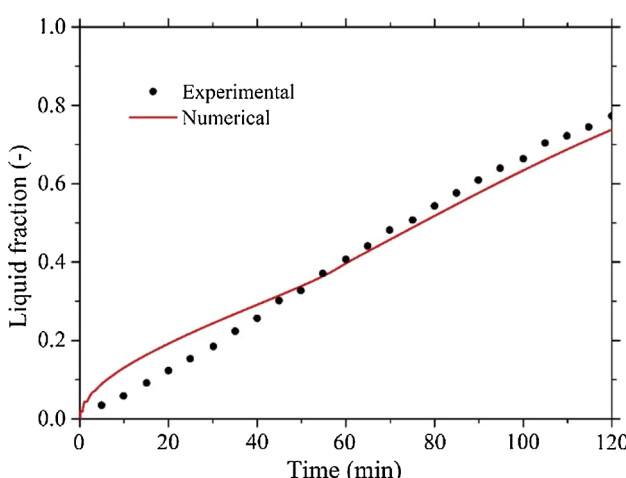


**Fig. 9.** Evolution of the liquid fraction.

treats the material as a porous medium. Porosity in each element is equal to the liquid fraction. The mushy zone (partial solidified region) is where the liquid fraction has a value between 0 and 1. When the material is fully solidified the liquid fraction becomes 0, which extinguishes the velocity in these regions. To make that possible, a sink term is added in momentum equation (Eq. (3)):

$$\vec{F} = \frac{(1-f)^2}{(f^3 + \varepsilon)} A_{mush} \vec{v} \quad (10)$$

Where  $\varepsilon$  is a small number (0.001) to prevent division by zero, and  $A_{mush}$  is the mushy zone constant. PCM thermic and hydraulic behavior is significantly influenced by the mushy zone parameter [15,43], it measures the amplitude of the damping; the higher this value, the steeper the transition of the velocity of the material to zero as it solidifies. Huge values of  $A_{mush}$  may cause the predicted solution to oscillate. In the present study,  $A_{mush}$  had a value of  $10^2$ .

To solve the mathematical model, based on the physical problem, the following initial condition was proposed:

$$\begin{aligned} T &= T_c \\ t = 0 \quad 0 \leq x \leq L_x + \delta \quad 0 \leq y \leq L_y \quad v_x &= 0 \\ v_y &= 0 \end{aligned}$$

With the following boundary conditions for  $t > 0$ :

$x = 0$	$0 \leq y \leq L_y$	$v_x = 0$
$x = L_x$	$0 \leq y \leq L_y$	$v_x = 0$
$x = L_x + \delta$	$0 \leq y \leq L_y$	$v_x = 0$
$0 \leq x \leq L_x + \delta$	$y = 0$	$v_x = 0$
$0 \leq x \leq L_x + \delta$	$y = L_y$	$v_x = 0$
$x = 0$	$0 \leq y \leq L_y$	$T = T_c$
$x = L_x$	$0 \leq y \leq L_y$	$T_{air} = T_{PCM}$
$x = L_x$	$0 \leq y \leq L_y$	$-\lambda_{air} \frac{\partial T}{\partial x} = -\lambda_{PCM} \frac{\partial T}{\partial x}$
$x = L_x + \delta$	$0 \leq y \leq L_y$	$-\lambda_{PCM} \frac{\partial T}{\partial x} = q''$
$0 \leq x \leq L_x + \delta$	$y = 0$	$\frac{\partial T}{\partial y} = 0$
$0 \leq x \leq L_x + \delta$	$y = L_y$	$\frac{\partial T}{\partial y} = 0$

To generalize the results, the Rayleigh, Nusselt, and Stefan dimensionless numbers were used, they were evaluated with the following relationships:

$$Ra_{air} = \frac{g \beta q' L_y^4}{\nu_{air} \alpha_{air} \lambda_{air}} \quad (11)$$

$$Nu_{air} = \frac{q_{convection}}{q_{conduction}} = \frac{h L_y}{\lambda_{air}} \quad (12)$$

$$Ste_{PCM} = \frac{\text{Sensible heat}}{\text{Latent heat}} = \frac{C_p l q'}{\lambda_l L} \quad (13)$$

where,  $g$  is the gravitational acceleration,  $h$  is the convective heat transfer coefficient,  $q''$  is the heat flux on the heated wall,  $\alpha$  is the thermal diffusivity,  $\beta$  is the volumetric thermal expansion coefficient,  $\lambda$  is the thermal conductivity,  $\nu$  is the kinematic viscosity,  $C_p$  is the specific heat,  $d$  is the PCM thickness, and  $L$  is the latent heat.

### 3. Experimental validation of the simulation model.

To validate the simulation model, an experimental prototype was built. The experimental system is shown in Fig. 2. In the air-filled cavity, to construct the walls 0.0125 m thickness medium density fiberboard (MDF) was used. Inside the cavity, all the surfaces were

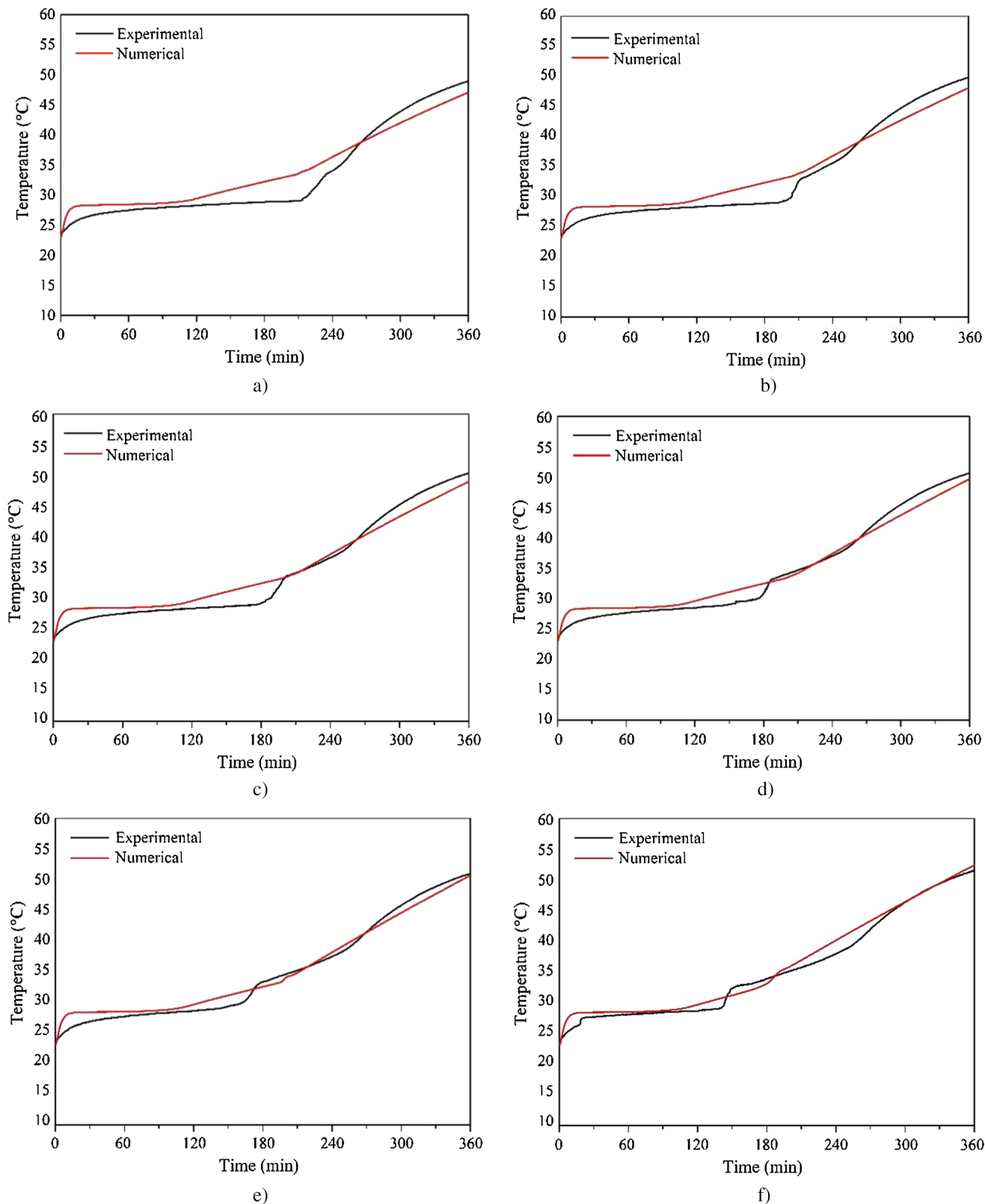


**Fig. 10.** Temporary evolution of the temperature at different points within the PCM a)  $X = 0.305\text{ m}$ ,  $Y = 0.1\text{ m}$ ,  $Z = 0.15\text{ m}$ , b)  $X = 0.305\text{ m}$ ,  $Y = 0.15\text{ m}$ ,  $Z = 0.15\text{ m}$ , c)  $X = 0.305\text{ m}$ ,  $Y = 0.2\text{ m}$ ,  $Z = 0.15\text{ m}$ , d)  $X = 0.305\text{ m}$ ,  $Y = 0.23\text{ m}$ ,  $Z = 0.15\text{ m}$ , e)  $X = 0.305\text{ m}$ ,  $Y = 0.26\text{ m}$ ,  $Z = 0.15\text{ m}$ , f)  $X = 0.305\text{ m}$ ,  $Y = 0.28\text{ m}$ ,  $Z = 0.15\text{ m}$ .

coated with a polished aluminum sheet to minimize thermal radiation; besides, the walls of the cavity were covered with 0.1 m of polystyrene as thermal insulation. On the other hand, the PCM filled cavity was built of two 0.005 m thickness aluminum sheets. One of its vertical

walls performed as the air-PCM interface while the other had a constant heat flux.

The constant heat flux was provided by an Omega brand flexible electrical heater, covered with silicon, and with dimensions of

**Table 3**

Differences between experimental and numerical temperatures in PCM.

Position (X = 0.305 m, Z = 0.15 m)						
	Y = 0.1 m	Y = 0.15 m	Y = 0.2 m	Y = 0.23 m	Y = 0.26 m	Y = 0.28 m
RMSE	1.76	1.79	1.80	1.48	1.31	0.99
MAPE	0.52%	0.53%	0.53%	0.44%	0.38%	0.28%

0.3 m × 0.3 m. It was connected to a VARIAC AC variable auto-transformer model 3PN1010B, allowing variate the electrical tension and obtaining the necessary thermal power. One side of the heater was in contact with PCM filled cavity, and the others were covered with 0.1 m of mineral wood. A TEMP-PLATE heat exchanger connected to Cole-Parmer thermostatic bath, with water as a thermal fluid, was used to keep the constant temperature in one of the air-filled cavity vertical walls.

The temperature measurement system consisted in 107 K-type thermocouples (which have an uncertainty of ± 0.5 °C), with a diameter of 0.079 mm (40 AWG) connected to two Agilent dataloggers model 34972A, with three multiplexor cards and twenty thermocouples capacity each. Eighty-five thermocouples were placed inside air filled cavity. They formed five temperature profiles along × coordinate (Fig. 3), on the following height and depths values: Y = 0.075 m, Z = 0.15 m; Y = 0.15 m, Z = 0.15 m; Y = 0.15 m, Z = 0.225 m; Y = 0.225 m, Z = 0.15 m; Y = 0.28 m, Z = 0.15 m. Every profile had seventeen thermocouples placed in the following position on the X-axis: 0.004 m, 0.008 m, 0.012 m, 0.016 m, 0.02 m, 0.03 m, 0.05 m, 0.1 m, 0.15 m, 0.2 m, 0.25 m, 0.27 m, 0.28 m, 0.284 m, 0.288 m, 0.292 m, 0.296 m. 6 thermocouples were located inside PCM filled cavity, to create a Y-axis profile at X = 0.305 and Z = 0.15, on the following heights: 0.1 m, 0.15 m, 0.2 m, 0.23 m, 0.26 m, 0.29 m. Fifteen thermocouples were located in air-PCM interface wall, on the following heights: Y = 0.275 m, Y = 0.15 m, Y = 0.075 m, Y = 0.01 m and at the following depths Z = 0.275 m, Z = 0.15 m, Z = 0.075 m. One thermocouple was placed at the center of the constant temperature wall (X = 0 m, Y = 0.15 m, Z = 0.15 m).

#### 4. Numerical procedure.

To solve the governing equations and obtain numerical results, commercial package ANSYS FLUENT v15 was used [44], which is based on the finite volume method to solve the equations. The PISO algorithm was used to couple momentum and continuity equations [45]. The convective terms were discretized applying the MUSCL scheme [46]. For time discretization a second-order implicit scheme was used. The convergence criteria, for each time step, was that the weighted residue in the energy equation was < 10<sup>-6</sup>, and the rest of the equations were < 10<sup>-3</sup>.

The proper mesh was chosen using a mesh independence study, with the following conditions: a constant heat flux of 250 W/m<sup>2</sup>, the isothermal wall was kept at 293.15 K, and a time step size of 0.75 s. Due to the geometry, a structured mesh consisting of rectangles was used (Fig. 4a). For the air part, a mesh size of 80x120 nodes was used, considering non-uniformity near the wall of constant temperature and in the proximity to the wall of the interface. The position of the first node was 0.0015 m from the interface and isothermal wall. For the PCM domain, the mesh size was 50x120 nodes with a uniform distribution. The spatial independence is shown in Fig. 4b); this shows the temporal evolution of the Nusselt number of the interface wall. The PCM mesh was varied from 20 to 60 nodes in the x-direction. For the meshes with 20, 30, and 40 nodes fluctuations are noticed in a specific part of the graph, which is why a mesh with 50 nodes was chosen as independent. For time step independence study, different time steps were used (0.1, 0.5, 0.75, 1, 2 s), the percentage error of the liquid fraction was

calculated, as well as the number of Nusselt in the interface. The time step was independent from 0.75 s with a percentage error of less than 1%, as it is shown in Table 1.

#### 5. Materials properties

The materials properties used in these simulations are shown in Table 2. PCM used were PureTemp 29X, whose appearance is transparent in liquid state and white in solid. Properties were taken from the datasheet provided by PureTemp™.

Density, thermal conductivity, and specific heat are temperature-dependent properties; therefore, in simulations, these properties are represented as liquid fraction function.

$$Cp = \begin{cases} Cp_s & T < T_s \\ Cp_s + (Cp_l - Cp_s)f & T_s < T < T_l \\ Cp_l & T > T_l \end{cases} \quad (14)$$

$$\rho = \begin{cases} \rho_s & T < T_s \\ \rho_s + (\rho_l - \rho_s)f & T_s < T < T_l \\ \rho_l & T > T_l \end{cases} \quad (15)$$

$$\lambda = \begin{cases} \lambda_s & T < T_s \\ \lambda_s + (\lambda_l - \lambda_s)f & T_s < T < T_l \\ \lambda_l & T > T_l \end{cases} \quad (16)$$

To obtain accurate numerical results, volume change from solid to liquid was taken into consideration [31]. During the phase change processes, the PCM expands, and the occupied height increases, as shown in Fig. 5.

The volume expansion of the PCM is calculated based on the mass conservation. If the top surface area is constant, then:

$$L * \rho_{PCM} = L \rho_l \quad (17)$$

Where L\* and L are actual and total PCM height, respectively, ρ<sub>PCM</sub> is the instantaneous PCM density, which is linked to the liquid fraction, and it is computed with Eq. (14). The L\* is given by:

$$L * = \frac{L}{(1-f)\frac{\rho_s}{\rho_l} + f} \quad (18)$$

And the occupied height by air:

$$\Delta L = L - L * \quad (19)$$

From the numerical point of view, to solve the expansion of the PCM, it is necessary to use a moving mesh along the Y-axis, but this would entail a great computational cost. Therefore, it was considered that the material had an effective density (ρ<sub>effective</sub>) given by the following equation:

$$\rho_{eff} = \rho_l + \frac{\Delta L}{L} \rho_{air} \quad (20)$$

#### 6. Discussion of results

##### 6.1. Verification of two-dimensional behavior

From the computational point of view, simplifying a three-

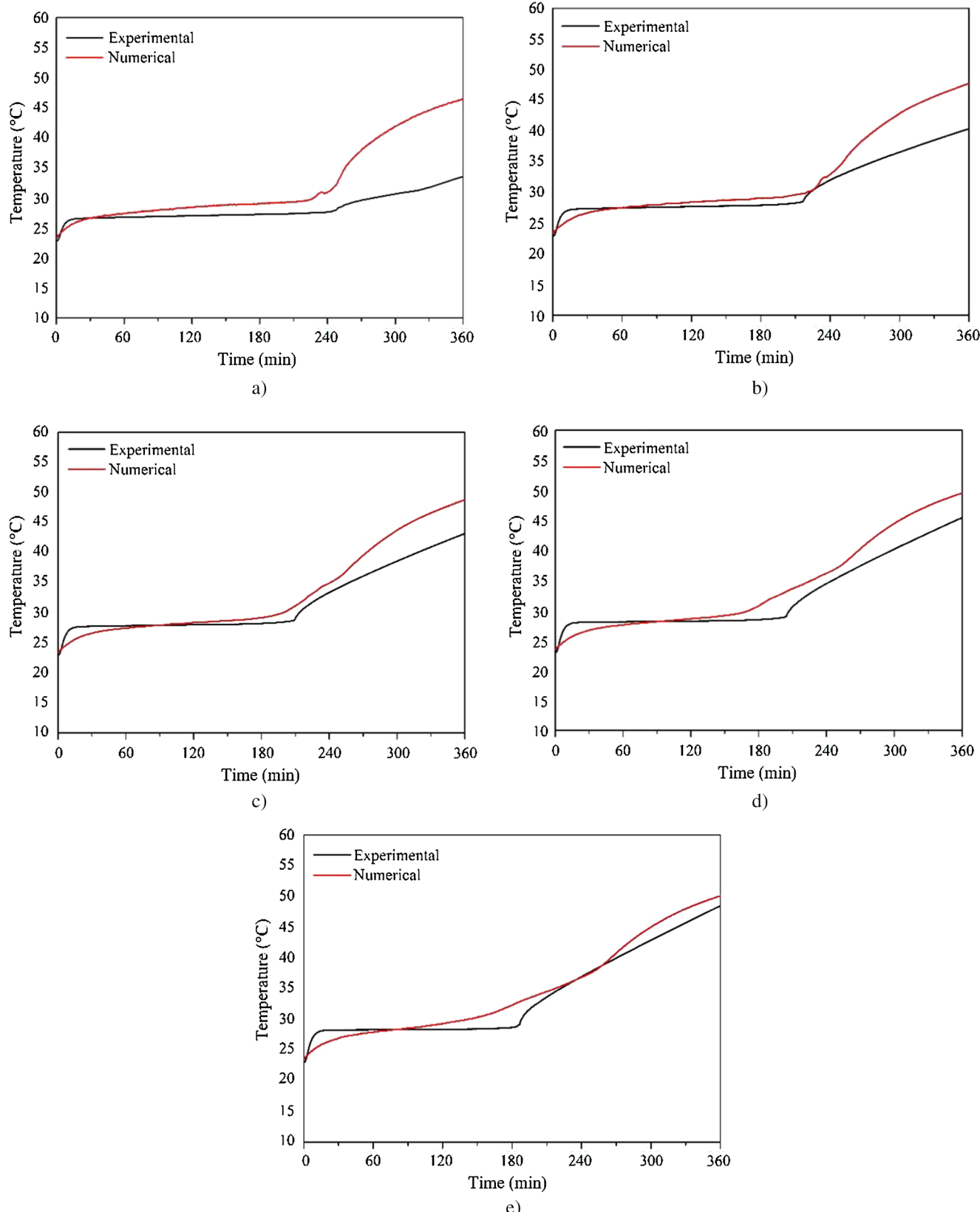


**Fig. 11.** Temporary evolution of the temperature at different points within the shared wall. a)  $X = 0.3 \text{ m}$ ,  $Y = 0.01 \text{ m}$ ,  $Z = 0.15 \text{ m}$ , b)  $X = 0.3 \text{ m}$ ,  $Y = 0.075 \text{ m}$ ,  $Z = 0.15 \text{ m}$ , c)  $X = 0.3 \text{ m}$ ,  $Y = 0.15 \text{ m}$ ,  $Z = 0.15 \text{ m}$ , d)  $X = 0.3 \text{ m}$ ,  $Y = 0.225 \text{ m}$ ,  $Z = 0.15 \text{ m}$ , e)  $X = 0.3 \text{ m}$ ,  $Y = 0.28 \text{ m}$ ,  $Z = 0.15 \text{ m}$ .

dimensional model to a two-dimensional model leads to considerable savings in computation time. That the present problem can be considered two-dimensional was a hypothesis that was considered at the

time of posing the governing equations. To validate this hypothesis, the experimental data obtained was used.

Fig. 6 shows the temporal evolution of each of the thermocouples,

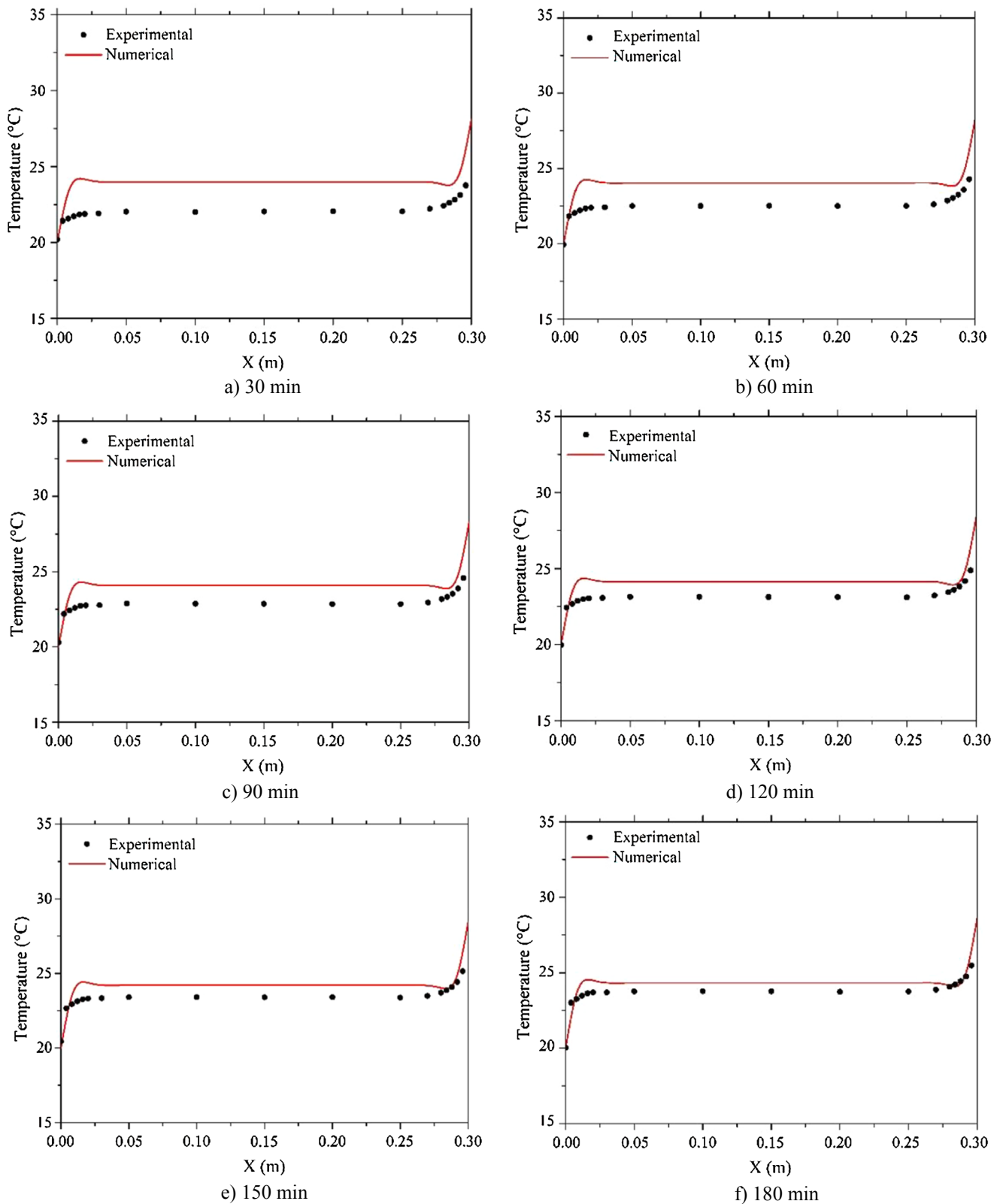


**Fig. 12.** Air temperature profiles ( $Y = 0.15 \text{ m}$ ,  $Z = 0.15 \text{ m}$ ). a) 30 min, b) 60 min, c) 90 min, d) 120 min, e) 150 min and f) 180 min.

which were in profiles at the same height but at different depth ( $Y = 0.15 \text{ m}$ ,  $Z = 0.15 \text{ m}$  and  $Y = 0.15 \text{ m}$ ,  $Z = 0.225 \text{ m}$ ). Very similar behavior is observed between both profiles. To quantify the difference between these, the root mean square error (RMSE) was calculated for each thermocouple, taking an average with respect to time; the

maximum value obtained was 0.38 and the minimum 0.14, with an average of 0.25. In Fig. 7, the temperatures in the interface wall for each time, each curve represents one of the four different heights, to which the thermocouples were placed. Each plot corresponds to one of the three different depths. There is no significant change in the graphs

**Table 4**  
Average absolute percentage error (%) in the profile  $Y = 0.15$  m.

Position (m)	Time (min)					
	30	60	90	120	150	180
0.296	0.80	0.65	0.57	0.50	0.43	0.35
0.292	0.52	0.39	0.31	0.23	0.16	0.09
0.288	0.39	0.26	0.18	0.10	0.03	0.05
0.284	0.40	0.27	0.19	0.11	0.04	0.04
0.28	0.47	0.34	0.25	0.18	0.11	0.03
0.27	0.59	0.48	0.38	0.30	0.24	0.15
0.25	0.66	0.52	0.42	0.35	0.28	0.19
0.2	0.65	0.52	0.42	0.34	0.27	0.20
0.15	0.66	0.51	0.42	0.34	0.27	0.19
0.1	0.67	0.52	0.42	0.34	0.27	0.18
0.05	0.66	0.52	0.41	0.34	0.27	0.19
0.03	0.71	0.56	0.45	0.37	0.29	0.22
0.02	0.77	0.62	0.51	0.43	0.35	0.27
0.016	0.80	0.65	0.53	0.46	0.39	0.31
0.012	0.78	0.63	0.52	0.44	0.37	0.30
0.008	0.59	0.44	0.33	0.26	0.19	0.12
0.004	0.15	0.02	0.09	0.16	0.22	0.32
0	0.06	0.02	0.10	0.01	0.15	0.01
Average	0.57	0.44	0.36	0.29	0.24	0.18

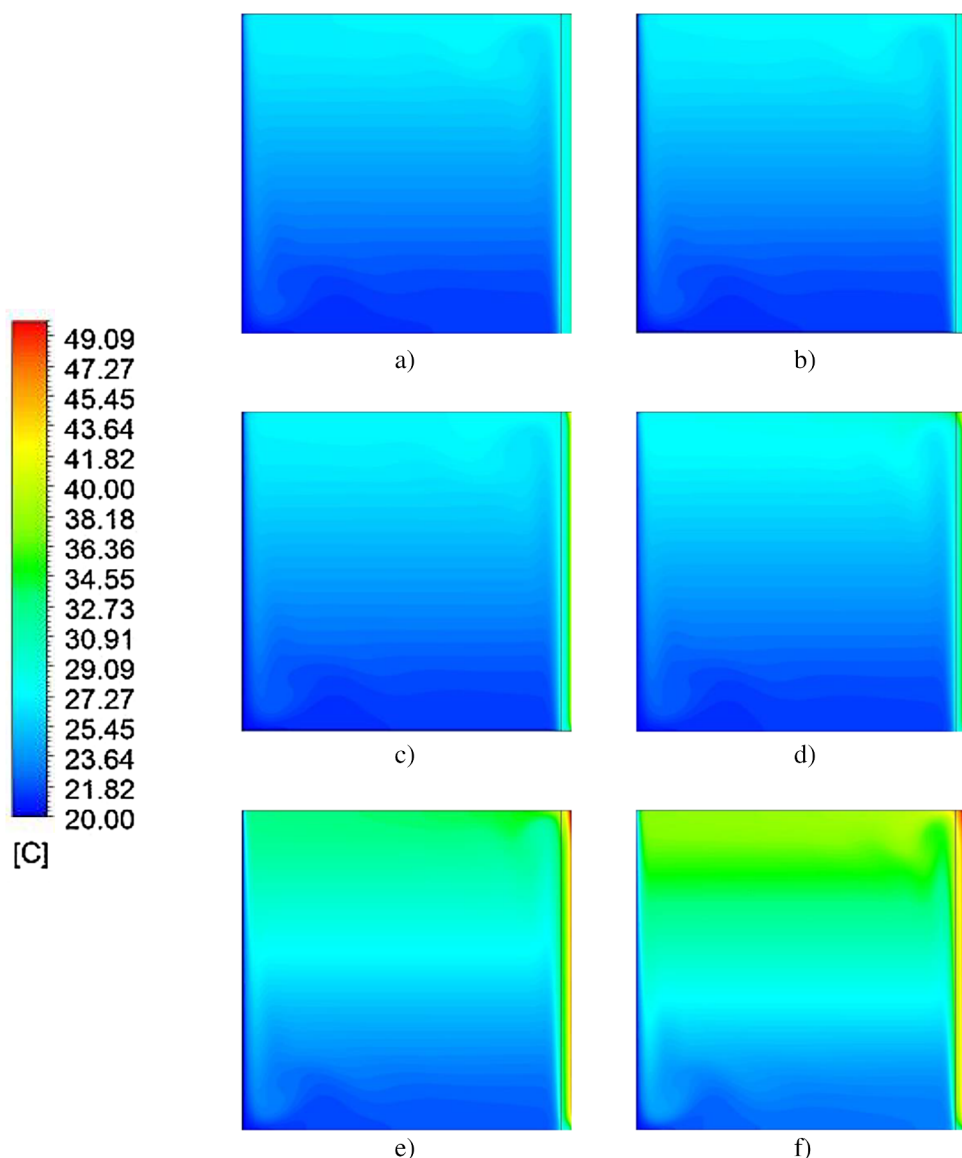


**Fig. 13.** Temperature contours for air a) 30 min, b) 60 min, c) 90 min, d) 120 min, e) 150 min, f) 180 min.

according to their depth. Given the above, it can be concluded that in this case study, a simplification to a two-dimensional model may be applicable.

## 6.2. Validation of the mathematical model for PCM

To demonstrate that the theoretical model can correctly simulate the fusion front, the results reported by Kamkari [21] were taken. For the comparison, the data obtained with a wall temperature of 70 °C and an inclination angle of 90° were used. The material used was lauric acid. For the simulation, a uniform unstructured mesh of  $100 \times 240$  elements was used, a time step of 0.5 s, and the mushy zone constant was given the value of  $10^2$ . In Fig. 8 is shown the comparison between the numerical results against the photographs obtained by Kamkari [21], which shows the front that forms the PCM at the time of being cast for different times (10, 20, 30, 40, 60 and 80 min). A good agreement was observed on the fronts. One difference was that for large times, such as 60 and 80 min, in the experiments a bit of molten material is noted in the lower right, while in the simulations that area was not noticed. Fig. 9 shows the evolution of the liquid fraction; a greater difference was observed during the first 40 min; after this, the values were very similar. The root mean square error (RMSE) was 0.03.

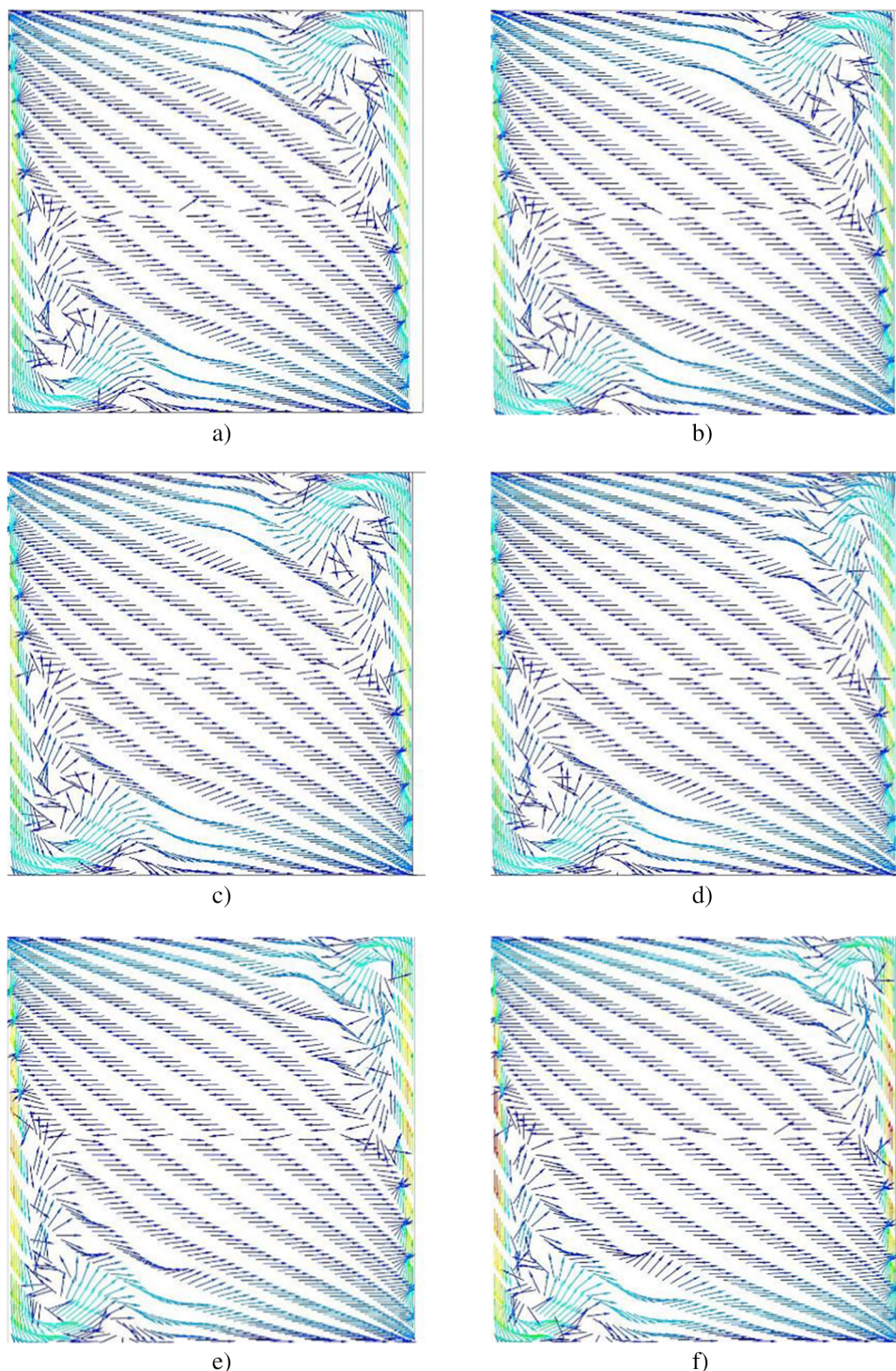


**Fig. 14.** Velocity vectors for air and PCM. a) 30 min, b) 60 min, c) 90 min, d) 120 min, e) 150 min, f) 180 min.

### 6.3. Validation of the coupled mathematical model for PCM and air

Fig. 10 shows the comparison of numerical and experimental temperatures within the PCM. We can see that the PCM started the process at a temperature lower than that of its phase change, so first, there is a heating stage, until reaching that temperature, in approximately 18 min. Subsequently, the PCM begins to function as an energy storage device, giving its phase change. Due to the convective effect, this stage lasts a different time for each height, since liquid density was lower than the solid. When the material has already changed its phase (liquid state), it goes to a stage of overheating in the PCM. From Table 3 and

Fig. 10, the temperature values in the three highest points were more accurate than in the other points. Graphically the highest point shows the most concordance; on the contrary, at the lowest point, a greater disagreement is noted. This because the model underestimated the time it takes for the PCM to change phase.

To compare the temperatures in the shared wall, an arithmetic average of the three thermocouples placed at the same height was made. Fig. 11 shows the comparison of evolution in time of temperatures in five heights of the shared wall. To quantify the error RMSE and mean absolute percentage error (MAPE) was used. Fig. 12 shows air temperature profiles for  $Y = 0.15$  m. For  $t = 30$  min, the mathematical

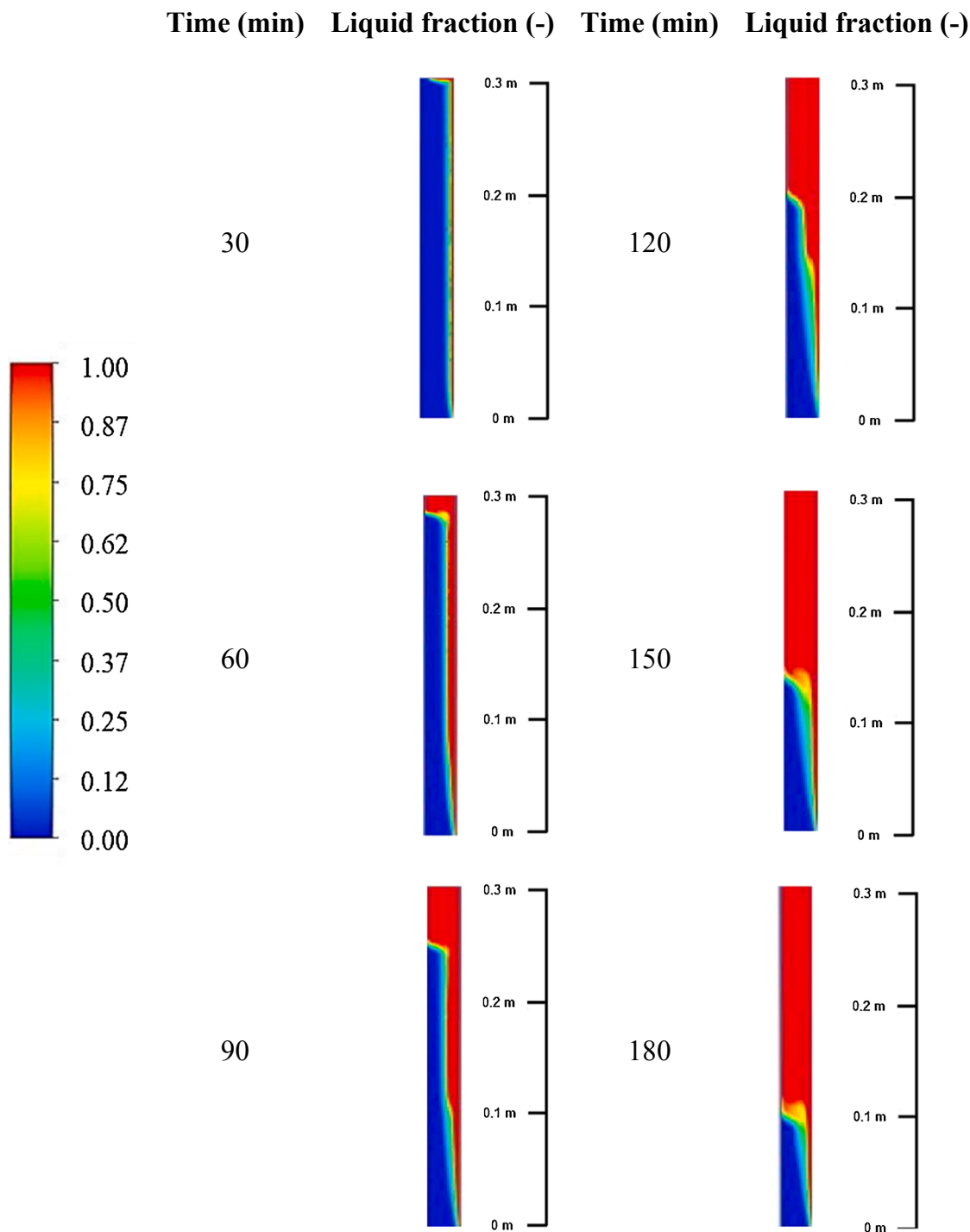


**Fig. 15.** Liquid fraction in PCM. a) 30 min, b) 60 min, c) 90 min, d) 120 min, e) 150 min, f) 180 min.

model overestimated the temperatures, but from  $t = 120$  min, the proximity between the experimental and numerical profiles is greater. This can be confirmed by looking at Table 4, which shows that the average percentage relative error at 30 min was 0.57% and decreased to 0.18% at 180 min.

#### 6.4. Numerical analysis

##### 6.4.1. Evolution of temperature field, flow pattern, and liquid fraction

Fig. 13 represents how the temperature field changes in both cavities; temperature contours are shown for every 30 min for 3 h. The hottest area is at the upper right corner, this due to the convective effect

that occurs in the PCM, causing that the liquid (which has a lower density) to go up and it is heated. Also, a temperature gradient along the Y coordinate is present in the interface wall. In the case of air, an almost uniform temperature can be seen for approximately the first 120 min. After this, the buoyancy force increases and moves up the hot air and causes that the upper part of the cavity is at a higher temperature than the lower part.

Fig. 14 shows the flow patterns in the air, for all times the behavior is very similar; the air rises due to flotation when heated on the interface wall, collides with the ceiling, continues its path, when it reaches the isothermal wall it is cooled and descends due to the same flotation effect, collides with the floor, and returns to where it started. The most

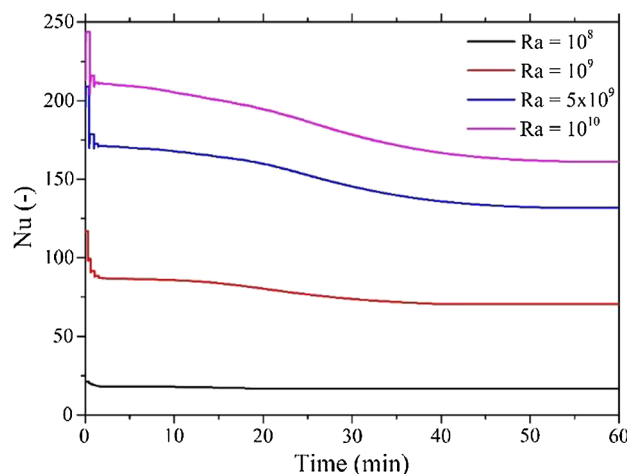


Fig. 16. Nusselt number evolution in the reference case.

**Table 5**  
Stefan number for different PCM thickness and heat fluxes.

Ra ( $\text{q}''$ )					
$\delta d$ (m)	$10^8$ ( $2.92 \text{ W}/\text{m}^2$ )	$10^9$ ( $29.16 \text{ W}/\text{m}^2$ )	$5 \times 10^9$ ( $145.81 \text{ W}/\text{m}^2$ )	$8.57 \times 10^9$ ( $250 \text{ W}/\text{m}^2$ )	$10^{10}$ ( $291.61 \text{ W}/\text{m}^2$ )
0.005	0.0009	0.0093	0.0467	0.0800	0.0934
0.01	0.0019	0.0187	0.0934	0.1601	0.1867
0.015	0.0028	0.0280	0.1400	0.2401	0.2801
0.02	0.0037	0.0373	0.1867	0.3201	0.3734

marked difference with increasing time is that the speed with which the air moves increases, this may be a consequence of the increase in the air temperature. The maximum velocity in the Y coordinate is preserved in the vicinity of the shared and isothermal walls. Another important aspect to consider is that in all the velocity vector figures, it is possible to appreciate what is known as a hydraulic jump in the upper right and lower left corners. In these walls, the air collides with higher speed, compared with the one that collides in the other two corners. It can be seen in the figures that the effect of the hydraulic jump is less pronounced as time increases.

In Fig. 15 is presented the fraction of liquid in the PCM for different times, blue mean solid, red mean liquid, and the area between them is the mushy zone. Every time, the material, that is closer to the heated

wall, is completely melted. The solidified material remained in the lower part of the cavity, and the PCM in the liquid state floated up, because of the buoyancy effect. During the 3 h, the phase change material did not change completely to a liquid state, but mostly.

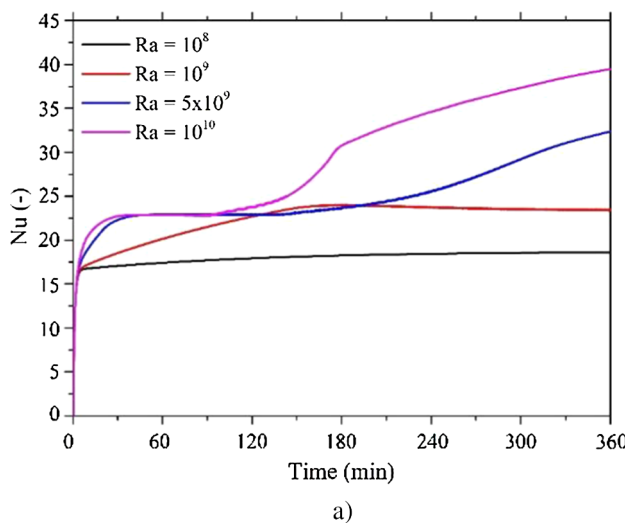
#### 6.4.2. Parametric study

A reference case was taken into consideration to determine how effective PCM is. In this case, a cavity without a PCM wall was used, it was exposed to a uniform constant heat flux. In Fig. 16 is seen the Nusselt number time evolution, it reaches a steady-state after 50 min for every Rayleigh number. It is shown that the Nusselt number is directly proportional to the Rayleigh number. Table 5 shows the heat flux imposed, as a boundary condition, in the hot wall to obtain each modified Rayleigh number. For reference case, Nusselt number was evaluated at the constant heat flux wall, meanwhile, for the case with PCM, it was evaluated at the shared wall.

Fig. 17a shows the influence of Rayleigh number on the Nusselt number of the shared wall. Since the PCM was solidified, it started storing latent heat; this causes that Nusselt number to remain constant in a lapse of time. Owing to density difference in liquid and solid PCM, the liquid went to the cavity upper part, and its temperature increased, that is why when most of PCM was molten Nusselt number increased too. For  $\text{Ra} = 10^{10}$  the increase of Nusselt number was at 90 min, according to Fig. 17b, at that time liquid fraction was 0.60. For  $\text{Ra} = 5 \times 10^9$  it happens at 145 min, when liquid fraction was 0.45, for Rayleigh  $10^9$  at 360 min where liquid fraction was 0.07, for this reason, Nusselt number did not suffer an increase. Besides using a PCM decrease the heat transfer. The comparison with reference case indicated that Nusselt number values reduced 75.47% for  $\text{Ra} = 10^{10}$ , 75.44% for  $\text{Ra} = 5 \times 10^9$  and 66.80% for  $\text{Ra} = 10^9$ .

Fig. 18a shows Nusselt number variation with time for different PCM thickness. On curves three sections are seen, the first one is when solid PCM reaches phase change temperature, and Nusselt number increases. The second is when the Nusselt number keeps at a constant value; it happens when phase change is in progress. The third one is when PCM is mostly molten, in this part heat transfer through PCM wall increase, as well as Nusselt number in the shared wall. Thicker PCM wall ensures a longer time-lapse that Nusselt number stays at a constant value, also after 360 min Nusselt number decrease from 43.65 in  $5 \times 10^{-4}$  thickness to 27.51 in  $2 \times 10^{-3}$  thickness. In Fig. 18b melting time for thicker PCM wall lasts longer, which occurs because it is more PCM mass.

The presence of the sharp bend is appreciated in Fig. 17b, for high Rayleigh numbers, and Fig. 18b, for low PCM wall thickness. This can



a)

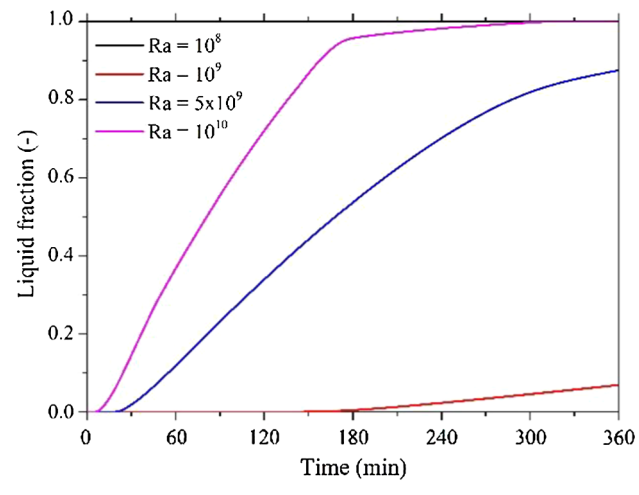
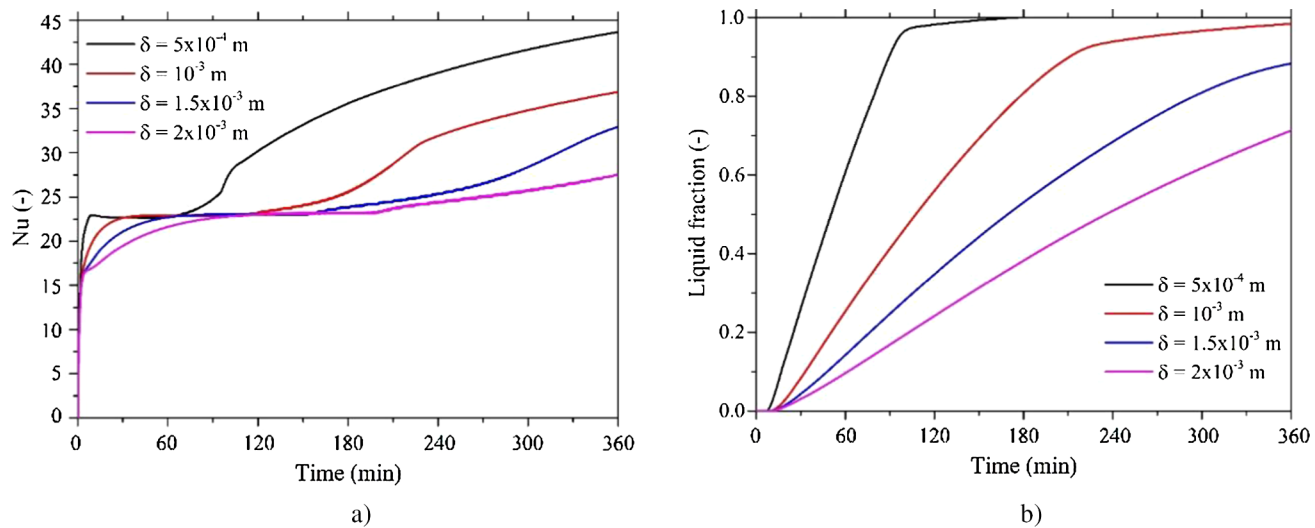
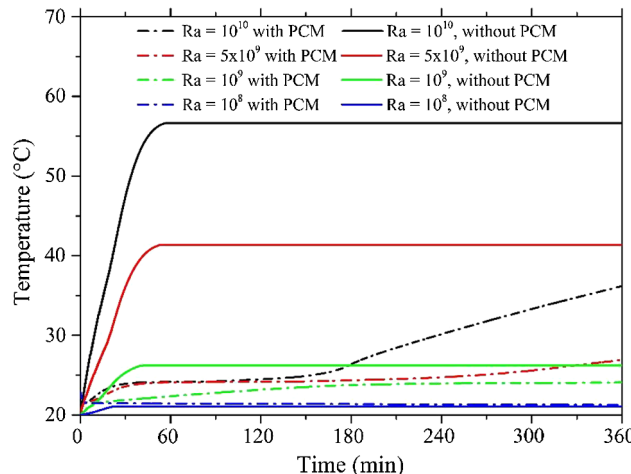


Fig. 17. Effect of Rayleigh number on evolution in time with ( $\delta = 10^{-3}$  m). a) Nusselt number, b) Liquid fraction.



**Fig. 18.** Effect of PCM thickness on evolution in time ( $Ra = 8.57 \times 10^9$ ). a) Nusselt number, b) Liquid fraction.



**Fig. 19.** Evolution in time of average air temperature with and without PCM.

be due to a small mass of PCM that remains in the bottom left of the cavity, which is in contact with the molten PCM but at the same time is being cooled with the air coming from the cold wall. This air temperature is under the phase change temperature; hence it is a resistance to the PCM to be completely molten.

Stefan number is a rough indicator of the ratio of sensitive to latent heat stored in the PCM. It was calculated and it is shown in Table 5, the increase of heat flux or PCM thickness is directly proportional to Stefan number. For all cases, Stefan number is smaller than 0.38 which means most of the heat is stored as latent heat.

An area weighed surface integral was used to calculate a mean temperature in the air cavity; this means temperature changes with time. Fig. 19 shows the mean temperature time evolution in the air cavity for the reference case and PCM thickness of  $10^{-3} \text{ m}$ . When there is not a PCM wall, steady-state is reached before 60 min for all Rayleigh numbers. When there is a PCM wall, air inside the cavity starts heating for about 30 min, then keeps at a constant temperature (meanwhile PCM is storing latent heat) for a time between 120 min ( $Ra = 10^{10}$ ) and 330 min ( $Ra = 10^8$ ). After that, for  $Ra > 5 \times 10^9$  (when most of the PCM is molten) air mean temperature rises again. After 360 min using a PCM wall, air mean temperature reduces from  $56^{\circ}\text{C}$  to  $36^{\circ}\text{C}$ ,  $41^{\circ}\text{C}$  to  $27^{\circ}\text{C}$  and  $26^{\circ}\text{C}$  to  $24^{\circ}\text{C}$ , for Rayleigh  $10^{10}$ ,  $5 \times 10^9$  and  $10^9$ , respectively. For Rayleigh  $10^8$ , no significant effect is observed, due to a small heat flux.

## 7. Conclusions

This paper reports a transient numerical and experimental study focused on describing the heat transfer in a cavity filled with air, which has one vertical wall with a phase change material (PCM). Numerical results were compared with experimental data. A parametric study was carried to see the impact of PCM thickness and different heat fluxes on heat transfer in the PCM and air. From the results, the following can be concluded:

1. For the theoretical study, the airflow inside the cavity was assumed to be two-dimensional. The assumption turned out to be adequate, observing that the experimental temperature data do not show significant differences between temperature profiles for different depths.
2. The comparison of numerical results with experimental data showed an overall relative percentage error of 0.48% for temperatures within the air cavity. On the other hand, for the temperatures in the PCM and the shared wall, this was 0.45% and 0.29%, respectively. This allows us to establish that the enthalpy method proved to be adequate to study the system proposed in this study.
3. Due to the buoyancy effect, the molten PCM generated a temperature gradient along the vertical direction, which caused an uneven temperature at the shared wall.
4. The use of the PCM decreased the heat transfer to the air. The comparison with the case without PCM indicated that Nusselt number values reduced between 66.80 and 75.47%.

## CRediT authorship contribution statement

**S. Moreno:** Software, Validation, Investigation, Writing - original draft, Writing - review & editing. **J.F. Hinojosa:** Conceptualization, Methodology, Writing - review & editing, Supervision, Funding acquisition. **I. Hernández-López:** Writing - review & editing, Visualization, Formal analysis. **J. Xaman:** Writing - review & editing, Visualization.

## Declaration of Competing Interest

The authors declare that they have no known competing financial interests or personal relationships that could have appeared to influence the work reported in this paper.

## Acknowledgement

**Funding:** The first author wishes to acknowledge the support of the National Council of Science and Technology (CONACYT of Mexico), given through its graduate scholarships program.

## References

- [1] D. of E. and S.A. United Nations, World Population Prospects: The 2017 Revision, (2017).
- [2] World Energy Council, World Energy Perspectives, (2014).
- [3] N.B. Geetha, R. Velraj, Passive cooling methods for energy efficient buildings with and without thermal energy storage - A review, (2012).
- [4] A. De Gracia, L.F. Cabeza, Phase change materials and thermal energy storage for buildings, *Energy Build.* 103 (2015) 414–419, <https://doi.org/10.1016/j.enbuild.2015.06.007>.
- [5] S.E. Kalnais, B.P. Jelle, Phase change materials and products for building applications: A state-of-the-art review and future research opportunities, Elsevier B.V. (2015), <https://doi.org/10.1016/j.enbuild.2015.02.023>.
- [6] K.O. Lee, M.A. Medina, E. Raith, X. Sun, Assessing the integration of a thin phase change material (PCM) layer in a residential building wall for heat transfer reduction and management, *Appl. Energy.* 137 (2015) 699–706, <https://doi.org/10.1016/J.APENERGY.2014.09.003>.
- [7] W.-B. Ye, Thermal and hydraulic performance of natural convection in a rectangular storage cavity, *Appl. Therm. Eng.* 93 (2016) 1114–1123, <https://doi.org/10.1016/J.APPLTHERMALENG.2015.10.083>.
- [8] N.S. Bondareva, M.A. Sheremet, Flow and heat transfer evolution of PCM due to natural convection melting in a square cavity with a local heater, *Int. J. Mech. Sci.* 134 (2017) 610–619, <https://doi.org/10.1016/J.IJMECSCI.2017.10.031>.
- [9] S. Li, Z. Sun, B. Xu, Y. Hong, Melting of phase change material from an isothermal vertical wall in a semi-enclosure, *Int. J. Heat Mass Transf.* 127 (2018) 1041–1052, <https://doi.org/10.1016/J.IJHEATMASSTRANSFER.2018.08.101>.
- [10] T. Bouhal, Z. Meghari, Saïf ed-Din Fertahi, T. El Rhafiki, T. Kousksou, A. Jamil, E. Ben Ghoulam, Parametric CFD analysis and impact of PCM intrinsic parameters on melting process inside enclosure integrating fins: Solar building applications, *J. Build. Eng.* 20 (2018) 634–646, <https://doi.org/10.1016/j.jobe.2018.09.016>.
- [11] Q. Wang, R. Wu, Y. Wu, C.Y. Zhao, Parametric analysis of using PCM walls for heating loads reduction, *Energy Build.* 172 (2018) 328–336, <https://doi.org/10.1016/j.enbuild.2018.05.012>.
- [12] M. Iten, S. Liu, A. Shukla, Experimental validation of an air-PCM storage unit comparing the effective heat capacity and enthalpy methods through CFD simulations, *Energy.* 155 (2018) 495–503, <https://doi.org/10.1016/J.ENERGY.2018.04.128>.
- [13] S. Li, N. Zhu, P. Hu, F. Lei, R. Deng, Numerical study on thermal performance of PCM Trombe Wall, *Energy Procedia.* 158 (2019) 2441–2447, <https://doi.org/10.1016/J.EGYPRO.2019.01.317>.
- [14] J. Xamán, R. Vargas-López, M. Gijón-Rivera, I. Zavala-Guillén, M.J. Jiménez, J. Arce, Transient thermal analysis of a solar chimney for buildings with three different types of absorbing materials: Copper plate/PCM/concrete wall, *Renew. Energy.* 136 (2019) 139–158, <https://doi.org/10.1016/J.RENENE.2018.12.106>.
- [15] M. Fadl, P.C. Eames, Numerical investigation of the influence of mushy zone parameter Amush on heat transfer characteristics in vertically and horizontally oriented thermal energy storage systems, *Appl. Therm. Eng.* 151 (2019) 90–99, <https://doi.org/10.1016/J.APPLTHERMALENG.2019.01.102>.
- [16] Y. Zhang, Modified computational methods using effective heat capacity model for the thermal evaluation of PCM outfitted walls, *Int. Commun. Heat Mass Transf.* 108 (2019) 104278, , <https://doi.org/10.1016/J.ICHEATMASSTRANSFER.2019.104278>.
- [17] F. Souyane, P.H. Biwole, F. Fardoun, Melting of a phase change material in presence of natural convection and radiation: A simplified model, *Appl. Therm. Eng.* 130 (2018) 660–671, <https://doi.org/10.1016/J.APPLTHERMALENG.2017.11.026>.
- [18] D.K. Bhamare, M.K. Rathod, J. Banerjee, Numerical model for evaluating thermal performance of residential building roof integrated with inclined phase change material (PCM) layer, *J. Build. Eng.* 28 (2020) 101018, , <https://doi.org/10.1016/j.jobe.2019.101018>.
- [19] H.M. Sadeghi, M. Babayan, A. Chamkha, Investigation of using multi-layer PCMs in the tubular heat exchanger with periodic heat transfer boundary condition, *Int. J. Heat Mass Transf.* 147 (2020) 118970, , <https://doi.org/10.1016/j.ijheatmasstransfer.2019.118970>.
- [20] S.A.M. Mehryan, K. Ayoubi-Ayoubloo, M. Shahabadi, M. Ghalambaz, P. Talebizadehsardari, A. Chamkha, Conjugate Phase Change Heat Transfer in an Inclined Compound Cavity Partially Filled with a Porous Medium: A Deformed Mesh Approach, *Transp. Porous Media.* 132 (2020) 657–681, <https://doi.org/10.1007/s11242-020-01407-y>.
- [21] B. Kamkari, H. Shokouhmand, F. Bruno, Experimental investigation of the effect of inclination angle on convection-driven melting of phase change material in a rectangular enclosure, *Int. J. Heat Mass Transf.* 72 (2014) 186–200, <https://doi.org/10.1016/J.IJHEATMASSTRANSFER.2014.01.014>.
- [22] X. Jin, M.A. Medina, X. Zhang, On the placement of a phase change material thermal shield within the cavity of buildings walls for heat transfer rate reduction, *Energy.* 73 (2014) 780–786, <https://doi.org/10.1016/j.energy.2014.06.079>.
- [23] N. Soares, A.R. Gaspar, P. Santos, J.J. Costa, Experimental evaluation of the heat transfer through small PCM-based thermal energy storage units for building applications, *Energy Build.* 116 (2016) 18–34, <https://doi.org/10.1016/J.ENBUILD.2016.01.003>.
- [24] Y.A. Kara, Diurnal performance analysis of phase change material walls, *Appl. Therm. Eng.* 102 (2016) 1–8, <https://doi.org/10.1016/j.applthermaleng.2016.03.141>.
- [25] X. Wang, H. Yu, L. Li, M. Zhao, Experimental assessment on the use of phase change materials (PCMs)-bricks in the exterior wall of a full-scale room, *Energy Convers. Manag.* 120 (2016) 81–89, <https://doi.org/10.1016/j.enconman.2016.04.065>.
- [26] A. Gounni, M. El Alami, The optimal allocation of the PCM within a composite wall for surface temperature and heat flux reduction: An experimental Approach, *Appl. Therm. Eng.* 127 (2017) 1488–1494, <https://doi.org/10.1016/J.APPLTHERMALENG.2017.08.168>.
- [27] H. Ambarita, I. Abdullah, C.A. Siregar, R.E.T. Siregar, A.D. Ronowikarto, Experimental Study on Melting and Solidification of Phase Change Material Thermal Storage, *IOP Conf. Ser. Mater. Sci. Eng.* 180 (2017) 12030, <https://doi.org/10.1088/1757-899x/180/1/012030>.
- [28] D. David, F. Kuznik, J.-J. Roux, Experimental investigation of natural convection near a wall containing phase change material, *Int. J. Therm. Sci.* 104 (2016) 281–291, <https://doi.org/10.1016/J.IJTHERMALSCI.2016.01.011>.
- [29] X. Sun, Y. Chu, Y. Mo, S. Fan, S. Liao, Experimental investigations on the heat transfer of melting phase change material (PCM), *Energy Procedia.* 152 (2018) 186–191, <https://doi.org/10.1016/J.EGYPRO.2018.09.079>.
- [30] X. Sun, Q. Zhang, M.A. Medina, K.O. Lee, Experimental observations on the heat transfer enhancement caused by natural convection during melting of solid-liquid phase change materials (PCMs), *Appl. Energy.* 162 (2016) 1453–1461, <https://doi.org/10.1016/J.APENERGY.2015.03.078>.
- [31] A. Labibhi, F. Aitlabib, H. Chehouani, B. Benhamou, M. Ouikhalfan, C. Croitoru, I. Nastase, Effect of phase change material wall on natural convection heat transfer inside an air filled enclosure, *Appl. Therm. Eng.* 126 (2017) 305–314, <https://doi.org/10.1016/J.APPLTHERMALENG.2017.07.112>.
- [32] H. Elarga, S. Fantucci, V. Serra, R. Zecchin, E. Benini, Experimental and numerical analyses on thermal performance of different typologies of PCMs integrated in the roof space, *Energy Build.* 150 (2017) 546–557, <https://doi.org/10.1016/J.ENBUILD.2017.06.038>.
- [33] M. Leporini, F. Corvaro, B. Marchetti, F. Polonara, M. Benucci, Experimental and numerical investigation of natural convection in tilted square cavity filled with air, *Exp. Therm. Fluid Sci.* 99 (2018) 572–583, <https://doi.org/10.1016/j.expthermflusci.2018.08.023>.
- [34] F. Corvaro, G. Nardini, M. Paroncini, R. Vitali, Piv and numerical analysis of natural convective heat transfer and fluid flow in a square cavity with two vertical obstacles, *Int. J. Heat Technol.* 33 (2015) 51–56, <https://doi.org/10.18280/ijht.330208>.
- [35] F. Corvaro, M. Paroncini, M. Sotte, PIV and numerical analysis of natural convection in tilted enclosures filled with air and with opposite active walls, *Int. J. Heat Mass Transf.* 55 (2012) 6349–6362, <https://doi.org/10.1016/j.ijheatmasstransfer.2012.06.003>.
- [36] M. Ghalambaz, A.J. Chamkha, D. Wen, Natural convective flow and heat transfer of Nano-Encapsulated Phase Change Materials (NEPCMs) in a cavity, *Int. J. Heat Mass Transf.* 138 (2019) 738–749, <https://doi.org/10.1016/j.ijheatmasstransfer.2019.04.037>.
- [37] A. Hajjar, S.A.M. Mehryan, M. Ghalambaz, Time periodic natural convection heat transfer in a nano-encapsulated phase-change suspension, *Int. J. Mech. Sci.* 166 (2020) 105243, , <https://doi.org/10.1016/j.ijmeccsci.2019.105243>.
- [38] S.A.M. Mehryan, M. Ghalambaz, A.J. Chamkha, M. Izadi, Numerical study on natural convection of Ag–MgO hybrid/water nanofluid inside a porous enclosure: A local thermal non-equilibrium model, *Powder Technol.* 367 (2020) 443–455, <https://doi.org/10.1016/j.powtec.2020.04.005>.
- [39] A.J. Chamkha, A. Doostanidezfuli, E. Izadpanahi, M. Ghalambaz, Phase-change heat transfer of single/hybrid nanoparticles-enhanced phase-change materials over a heated horizontal cylinder confined in a square cavity, *Adv. Powder Technol.* 28 (2017) 385–397, <https://doi.org/10.1016/j.japt.2016.10.009>.
- [40] V.R. Voller, M. Cross, N.C. Markatos, An enthalpy method for convection/diffusion phase change, *Int. J. Numer. Methods Eng.* 24 (1987) 271–284, <https://doi.org/10.1002/nme.1620240119>.
- [41] A.D. Brent, V.R. Voller, K.J. Reid, Enthalpy-porosity technique for modeling convection-diffusion phase change: Application to the melting of a pure metal, *Numer. Heat Transf. 13 (1988) 297–318*, <https://doi.org/10.1080/1040778808913615>.
- [42] V.R. Voller, L. Shadabi, Enthalpy methods for tracking a phase change boundary in two dimensions, *Int. Commun. Heat Mass Transf.* 11 (1984) 239–249, [https://doi.org/10.1016/0735-1933\(84\)90040-X](https://doi.org/10.1016/0735-1933(84)90040-X).
- [43] M. Kumar, D.J. Krishna, Influence of Musky Zone Constant on Thermohydraulics of a PCM, *Energy Procedia.* 109 (2017) 314–321, <https://doi.org/10.1016/J.EGYPRO.2017.03.074>.
- [44] ANSYS Inc. (USA), ANSYS Fluent Theory Guide, in: Canonsburg, PA, 2013: pp. 565–572.
- [45] R. Issa, Solution of the implicitly discretised fluid flow equations by operator-splitting, *J. Comput. Phys.* 62 (1986) 40–65, [https://doi.org/10.1016/0021-9991\(86\)90099-9](https://doi.org/10.1016/0021-9991(86)90099-9).
- [46] B. van Leer, Towards the ultimate conservative difference scheme. V. A second-order sequel to Godunov's method, *J. Comput. Phys.* 32 (1979) 101–136, [https://doi.org/10.1016/0021-9991\(79\)90145-1](https://doi.org/10.1016/0021-9991(79)90145-1).